Covariance-driven Stochastic Subspace Identification of an End-supported Pontoon Bridge Under Varying Environmental Conditions

Knut Andreas Kvåle, PhD Student, Department of Structural Engineering, Faculty of Engineering Science and Technology, NTNU, Norwegian University of Science and Technology, Trondheim, Norway
Ole Øiseth, Associate Professor, Department of Structural Engineering, Faculty of Engineering Science and Technology, NTNU, Norwegian University of Science and Technology, Trondheim, Norway
Anders Rönnquist, Professor, Department of Structural Engineering, Faculty of Engineering Science and Technology, NTNU, Norwegian University of Science and Technology, Trondheim, Norway

ABSTRACT
The Bergsøysund Bridge is currently being extensively monitored with accelerometers, anemometers, wave radars and GNSS sensors. By applying Covariance-driven Stochastic Subspace Identification (Cov-SSI), the modal parameters of the bridge are estimated. The results are interpreted in the context of the environment, represented by significant wave heights. The problem is characterized by the fact that modes are closely spaced in frequency and have high damping. Two weighting algorithms for the Cov-SSI are applied, to assess their performance for application on structures with these characteristics.

Keywords: floating bridge, stochastic subspace identification, environmental influence, wave excitation, high damping

Introduction

For decades, floating bridges served mainly as a military asset, for temporary crossings of rivers and straits. Floating bridges were first applied as critical links in modern road networks in the middle of the 20th century, with exception of the Galata floating bridge in Istanbul finished in 1912 [1]. The continuous box girder design has shown great success in the State of Washington, USA, where most of the existing floating bridges are located. For straits highly affected by current and wave action, floating bridges relying on separate and discretely distributed pontoons may be beneficial. By using such a design, the waves will excite the structure merely in the points where the pontoons are located, and the correlation of the excitation will influence the response in a manner more sensitive to changes in the wave field. This will be of particular importance when the spans of the bridges increase. Currently, limited experience about the behavior of such floating bridges is available, and a thorough study of existing structures will be valuable. There exist only two end-supported floating bridges in the world that rely on discretely distributed pontoons, both located in Norway. The Bergsøysund Bridge is one of them, and it is currently extensively monitored to study its behavior upon wave and wind excitation. Operational modal analysis (OMA) is a highly valuable tool in the study of the behavior of the bridge. The covariance-driven stochastic subspace identification (Cov-SSI) algorithm is amongst the methods considered most robust and accurate [2–5] and performs very well for traditionally tested civil structures, such as suspension bridges and high-risers. The performance of the Cov-SSI algorithm applied on the Bergsøysund Bridge has previously been studied by [6, 7]. In the current study, it is applied on recordings of acceleration of the bridge, to evaluate how it is affected by variations in the environmental conditions. The performances of various weighting algorithms are also assessed. The results are compared with modal parameters obtained from the eigenvalue solution of an model-updated version of the numerical prediction model presented in [8].

Covariance-driven Stochastic Subspace Identification

The applied implementation of the Cov-SSI algorithm is based on the description given by Herman and van Der Auweraer [9], and the reader is referred to the mentioned paper for specifics. Only the most important details are repeated here. The starting

point for the analysis is the block-Hankel matrix, $[H_i]$, which is constructed with sub-matrices representing the correlation between all the measurement channels l, with varying time shifts, as follows:

$$[H_i] = \begin{bmatrix} [R_1] & [R_2] & \dots & [R_i] \\ [R_2] & [R_3] & \dots & [R_{i+1}] \\ \vdots & \vdots & \ddots & \vdots \\ [R_i] & [R_{i+1}] & \dots & [R_{2i+1}] \end{bmatrix} \tag{1}$$

Here, $2i$ corresponds to the maximum number of time lags, or equally valid, i corresponds to the number of block rows. The correlation matrices are formally defined as:

$$[R_k] = \mathrm{E}\left(\{y_{n+k}\}\{y_n\}^T\right) \tag{2}$$

where the vector $\{y_n\}$ corresponds to the monitored quantities (accelerations) from all channels, for sample n. The sample-shift k is related to the time lag through $\Delta t = k f_s^{-1}$, where f_s is the sampling rate and Δt represents the time lag. The cross-correlation matrices may be efficiently computed based on FFT and IFFT, as is how the `xcorr` function built-in to MATLAB is functioning.

The block-Hankel matrix can be decomposed into the corresponding observability and controllability matrices as follows:

$$[H_i] = [\mathscr{O}_i][\mathscr{C}_i] \tag{3}$$

which further are defined as follows:

$$[\mathscr{O}_i] = \begin{bmatrix} [C] \\ [C][A] \\ [C][A]^2 \\ \vdots \\ [C][A]^{i-1} \end{bmatrix}, \qquad [\mathscr{C}_i] = \begin{bmatrix} [G] & [A][G] & \dots & [A]^{i-1}[G] \end{bmatrix} \tag{4}$$

The matrices $[A]$ and $[C]$ refer to the discrete state matrix and discrete output matrix, respectively, from the stochastic state space model describing the problem:

$$\{z_{n+1}\} = [A]\{z_n\} + \{w_n\} \tag{5}$$

$$\{y_n\} = [C]\{z_n\} + \{v_n\} \tag{6}$$

where $\{z_n\}$, $\{y_n\}$, $\{w_n\}$, and $\{v_n\}$ correspond to the state vector, output vector, process noise and measurement noise, respectively. The matrix $[G]$ is formally defined as follows:

$$[G] = \mathrm{E}\left(\{z_{n+1}\}\{y_n\}^T\right) \tag{7}$$

After pre-multiplication with $[W_1]$ and post-multiplication with $[W_2]^T$, the block-Hankel matrix is decomposed using singular value decomposition (SVD), and thereafter truncated, as follows:

$$[W_1][H_i][W_2]^T = \begin{bmatrix} [U_1] & [U_2] \end{bmatrix} \begin{bmatrix} [\Sigma_1] & [0] \\ [0] & [\Sigma_2] \end{bmatrix} \begin{bmatrix} [V_1]^T \\ [V_2]^T \end{bmatrix} \tag{8}$$

$$\approx \begin{bmatrix} [U_1] & [U_2] \end{bmatrix} \begin{bmatrix} [\Sigma_1] & [0] \\ [0] & [0] \end{bmatrix} \begin{bmatrix} [V_1]^T \\ [V_2]^T \end{bmatrix} \tag{9}$$

$$= [U_1][\Sigma_1][V_1]^T \tag{10}$$

The truncation above represents an approximation due to noise and imperfections in the system; a system of finite order will have non-zero values for $[\Sigma_2]$ in practice, and a manual specification of the order has to be made. The optimal order is not known a priori, and a stabilization plot is used to distinguish physical poles from spurious ones, using multiple truncation levels (orders). A pole is deemed physical and stable, as opposed to spurious and unstable, if certain criteria for deviance of modal quantities are fulfilled. One possible implementation of this is discussed in the sub-section below.

By combining Equation 3 and 8, the following estimate of the observability matrix is established:

$$[\mathscr{O}_i] = [W_1]^{-1}[U_1][\Sigma_1]^{1/2} \tag{11}$$

Then, the state matrix can be computed as follows:

$$[A] = [\mathscr{O}_{\text{down}}]^{\dagger}[\mathscr{O}_{\text{up}}] \tag{12}$$

where the matrices $[\mathscr{O}_{\text{down}}]$ and $[\mathscr{O}_{\text{up}}]$ both are subsets from $[\mathscr{O}_i]$, without the first or last l rows, respectively, and $\dagger$ denotes the pseudo-inverse. The output matrix $[C]$ is required to establish the physical mode shapes, and is retrieved from the first l rows of the observability matrix, as follows:

$$[C] = [\mathscr{O}_i]_{1:l} \tag{13}$$

By performing an eigenvalue decomposition of the discrete state matrix $[A]$, the discrete eigenvalues $\hat{\lambda}_r$ and the system eigenvectors $[\Psi]$ are established, which thereafter are transformed to continuous eigenvalues and to eigenvectors with coordinates referring to the sensor coordinates as follows:

$$\lambda_r = \ln\left(\hat{\lambda}_r\right) \cdot f_s^{-1}, \quad [\Phi] = [C][\Psi] \tag{14}$$

where the modal transformation matrix $[\Phi]$ has columns that refer to the identified mode shapes $\{\phi_r\}$, where r is the mode index.

Selection of weighting matrices

There are two traditional selections for the weighting matrices $[W_1]$ and $[W_2]$ for Cov-SSI, namely the canonical variate analysis (CVA) weighting and the balanced realization (BR) weighting.

The CVA weighting is commonly interpreted as the weights ensuring balanced energy levels for all the system modes (see e.g. [9]). The following two Toeplitz-structured matrices are used as a starting point:

$$[R^+] = \begin{bmatrix} [R_0] & [R_1]^T & \dots & [R_{i-1}]^T \\ [R_1] & [R_0] & \dots & [R_{i-2}]^T \\ \vdots & \vdots & \ddots & \vdots \\ [R_{i-1}] & [R_{i-2}] & \dots & [R_0] \end{bmatrix}, \qquad [R^-] = \begin{bmatrix} [R_0] & [R_1] & \dots & [R_{i-1}] \\ [R_1]^T & [R_0] & \dots & [R_{i-2}] \\ \vdots & \vdots & \ddots & \vdots \\ [R_{i-1}]^T & [R_{i-2}]^T & \dots & [R_0]^T \end{bmatrix} \tag{15}$$

The weights are thereafter defined as follows:

$$[W_1] = [L^+]^{-1}, \quad [W_2] = [L^-]^{-1} \tag{16}$$

where $[L^+]$ and $[L^-]$ are established from the Cholesky decomposition of $[R^+]$ and $[R^-]$, respectively. This weighting is reported to yield a better identification of less excited modes. The Cholesky decomposition is not straightforward to perform due to the poor conditioning of the input matrices. The authors observed that the block-Cholesky decomposition algorithm described in [10], modified to use Gaxpy-rich Cholesky factorization, was rather robust.

BR weighting is analogous to using unit matrices for $[W_1]$ and $[W_2]$.

Efficient stabilization analysis

To determine if poles corresponding to analyses with different orders corresponds to the same mode, a modal indicator is used, which in the current study is the modal assurance criterion (MAC) number. The MAC number between poles p and q are computed as follows:

$$\text{MAC}_{p,q} = \frac{|\{\phi_q\}^T\{\phi_p\}|^2}{\{\phi_q\}^T\{\phi_q\} \cdot \{\phi_p\}^T\{\phi_p\}} \tag{17}$$

where the $\bar{\cdot}$ is the complex conjugate operator. The poles from the current order are identified to correspond to the poles from the previous order by finding the maximum value of the MAC between the poles in the different orders. The most common choice for a modal indicator is the frequency, but because the modes are closely spaced in frequency, the MAC number is a better choice for the current study. For a pole from a analysis with a higher order to be considered stable, it has to fulfill the following criteria when compared to a previous reference pole: it has to deviate a maximum amount in frequency and damping, and their mode shapes have to yield a MAC value above a certain threshold. To increase the clarity of the stabilization plots, the parameter *stability level* is introduced. For a stability level of s, the above requirements have to be fulfilled with all poles corresponding to calculations with 1-s orders lower than the queried pole.

Figure 1: The Bergsøysund Bridge. Photograph by NTNU/K. A. Kvåle.

Table 1: Vital statistics of the selected recording, initiated 06:47 on December 26, 2015, with a duration of 30 minutes. The indicated wind direction corresponds to the angle of origin of the wind, where 0° corresponds to winds along the x-axis indicated in Figure 2 and increases in an clockwise manner.

	Waves		Horizontal wind		Acceleration*	
Position	SWH [cm]	Pontoon water level [cm]	Speed [m/s]	Direction [°]	Lateral [mg]	Vertical [mg]
Center (pontoon 4)	34.8	407	12.4	264.7	1.8	0.5
Quarter (pontoon 2)	-	-	12.3**	262.7**	1.4	0.5

* g is used as acceleration unit, and refers to the gravitational constant ($g = 9.81 m/s^2$).

** Reported wind statistics refer to anemometer A1, positioned close to pontoon 2. See Figure 2.

The Bergsøysund Bridge

The Bergsøysund Bridge is a pontoon bridge with total length 931 m and main span 845 m, located on the northwestern coast of Norway. It consists of a steel truss supported by 7 concrete pontoons (Figure 1). The bridge is arc-shaped to reduce the bending moments due to lateral wave forces. The bridge is only supported in the ends, as no side-mooring is present. An extensive monitoring system is currently operating on the bridge (Figure 2). Three-dimensional anemometers are capturing winds 7 meters above the deck level at locations spread across the deck, while wave radars are monitoring the sea surface elevation near the center of the bridge. Furthermore, the response of the bridge is measured by means of two triaxial accelerometers on each pontoon and a single Global Navigation Satelite Systems (GNSS) displacement sensor located at midspan on top of the deck. The reader is referred to Kvåle et al. [11] for a more in-detail description of the monitoring system.

Operational Modal Analysis

The following stability criteria were used: maximum frequency deviance of 1%, maximum damping deviance of 5%, and a minimum MAC value of 95%. The stability level was chosen as $s = 8$ for the analyses of which all presented results are based on. By investigating the statistical properties of captured recordings, a suitable time series was identified. In particular, a recording with perpendicular winds and decent excitation levels was sought after. A recording made 06:47 on December 26, 2015, fits these requirements. Some vital statistics related to this recording are found in Table 1. Modal analyses were performed both with BR and CVA weighting. The resulting stabilization plots are shown in Figure 3, for both cases. It is clear that the CVA weighting does help in identifying the less excited modes for the current analysis. However, it is observed to behave rather erratically, and is very sensitive to input parameters, such as the number of block rows. The agreement with an updated version of the numerical prediction model in [8] is indicated with lines in the stabilization plot from the CVA analysis. To assess the effect of the increased stability level ($s = 8$), the stabilization plot from the analysis with CVA weighting is also shown wiht $s = 1$ in Figure 4. Increased stability level results in a better readability and clarity of the stabilization plot. Table 2 shows the modal parameters of the CVA analysis together with modal parameters obtained from the eigenvalue solution of

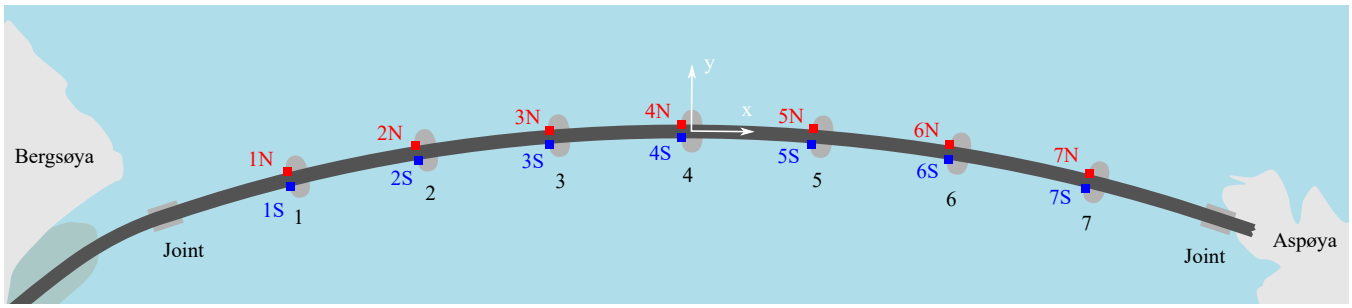

(a) Top view, including coordinate system definition.

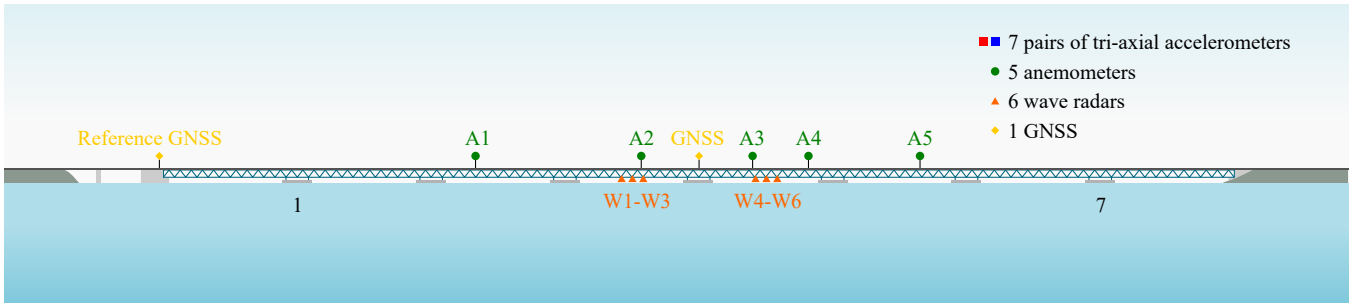

(b) Side view.

Figure 2: Monitoring system.

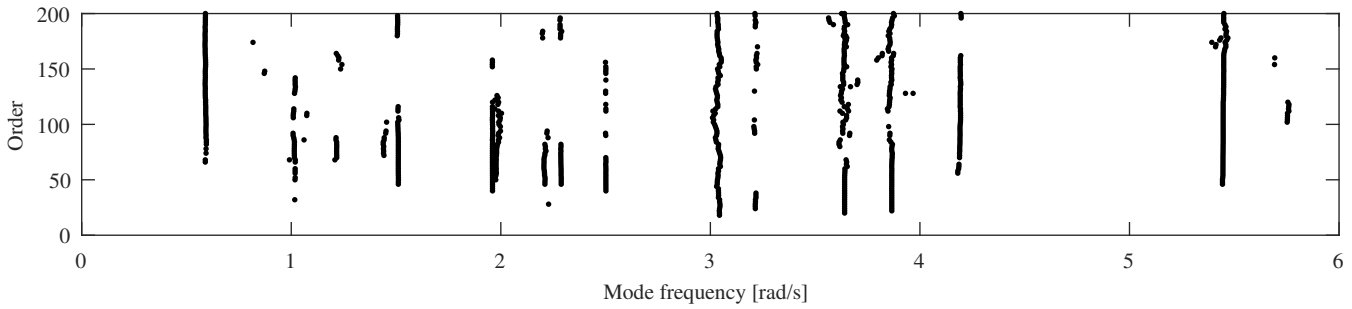

(a) BR weighting.

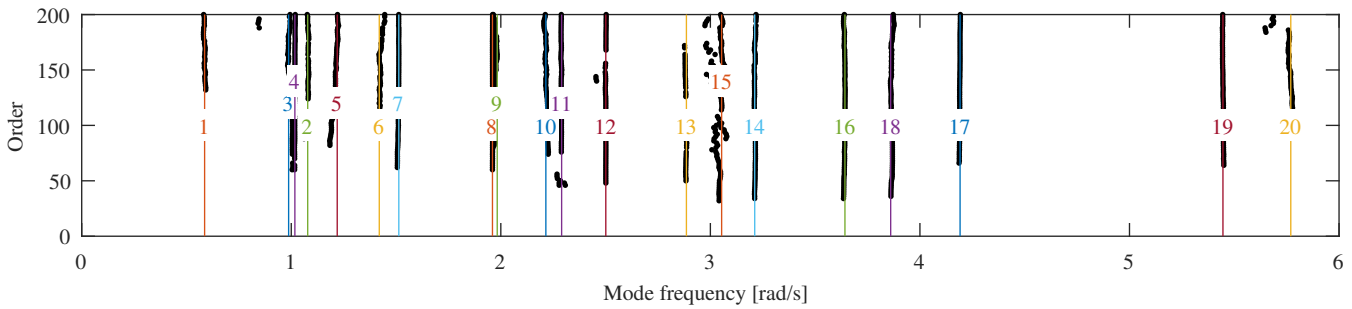

(b) CVA weighting. The lines indicate identified modes, with numbers corresponding to the modes from the numerical prediction model.

Figure 3: Stabilization plot from Cov-SSI analyses of the selected recording. Stabilization level $s = 8$.

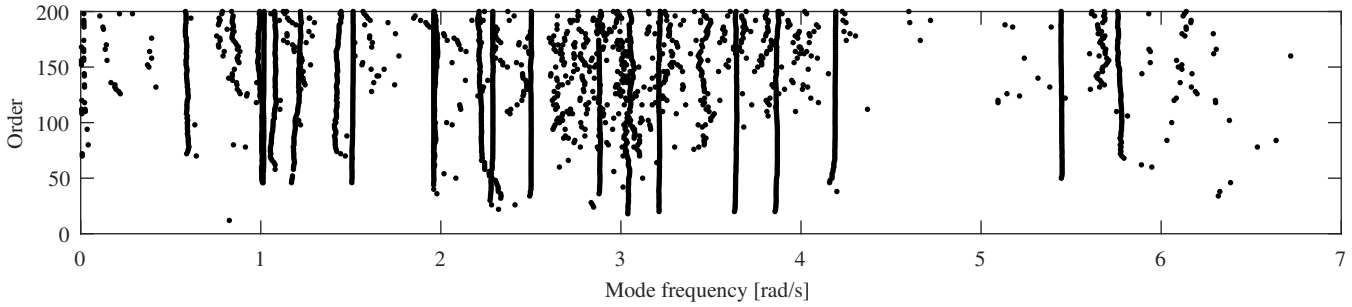

Figure 4: Stabilization plot from Cov-SSI analysis of the selected recording with CVA weighting. Stabilization level $s = 1$.

Table 2: Identified modal parameters compared with modal parameters from eigenvalue solution of numerical prediction model.

	Natural frequency, ω_r [rad/s]		Damping ratio, ξ_r [%]		
Mode number	Prediction	Cov-SSI/CVA	Prediction	Cov-SSI/CVA	MAC
1	0.58	0.59	1.63	5.16	0.94
2	0.99	1.08	12.25	4.47	0.32
3	1.03	0.99	11.24	11.62	0.86
4	1.05	1.02	5.00	2.53	0.53
5	1.17	1.22	7.67	4.88	0.95
6	1.38	1.42	5.91	6.93	0.78
7	1.44	1.51	3.28	2.65	0.98
8	1.87	1.96	1.07	0.96	0.67
9	1.95	1.98	3.62	3.15	0.90
10	2.23	2.21	0.43	1.86	0.89

the numerical prediction model. The corresponding mode shape comparison is found in Figure 5. Overall, a decent agreement is observed. The damping levels are not satisfactory, especially for modes 2, 4 and 5. The next sub-section indicates large variability of the damping ratios. Because the modes are closely spaced, they are prone to switch their ordering in frequency with small changes in the excitation. Furthermore, the complex, coupled and environment-dependent dynamic behavior is believed to make the appearance of the mode shapes more variable.

Automatic OMA and the effect of varying environment

By using the eigenvalue solution from the predictive numerical model as reference, the natural frequencies and critical damping ratios are automatically identified for various environmental conditions. The numerical prediction model is described in [8]. The MAC numbers between the predicted and measured mode shapes were required to have a value above 0.7, for storing as an identified mode. For the automatic OMA, the BR weighting is utilized due to higher robustness than the CVA weighting. The natural frequency and critical damping coefficients of mode 1, 2 and 3 are compared to the significant wave height (SWH) in Figure 6. The SHW is defined as $H_s = 4\sigma_\eta$, where σ_η is the standard deviation of the wave elevation process. Large variability in the modal parameters, in particular the damping ratios, are observed. The plots indicate that the damping ratio is increasing for increased SWH. Increased SWH affects the three presented natural frequencies differently. Furthermore, the scatter of the natural frequencies are reduced for increasing SWH, i.e., increased excitation levels. This tendency is explained by the fact that a larger amount of the excitation is accounted for when the SWH is larger.

Concluding remarks

The Cov-SSI method is successfully applied with different weighting schemes on the Bergsøysund Bridge, an end-supported pontoon bridge in current operation, to identify the structure's modal parameters. Damping ratios and MAC-values are poor for certain modes. The CVA weighting scheme improves the clarity of the stabilization plot to a great extent. When the CVA weighting is used in conjunction with a high stability level, the resulting stabilization plots become quite clear. On the other hand, the CVA weighting implementation used is observed as very sensitive to the input time series and parameters, and less robust than an unweighted analysis, i.e., BR weighting. The OMA procedure is made automatic by using the eigenvalue solution from a predictive numerical model as reference, which shows that the bridge's natural frequencies' variability is reduced when the excitation, represented by the SWH, is increased. Both mean value and variance of the damping ratios are in general increased as a consequence of increasing SWH.

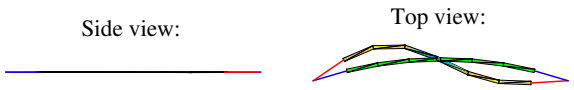

(a) Mode 1: numerical prediction.

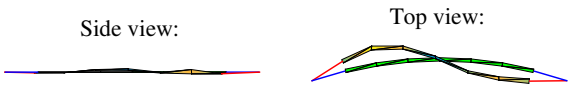

(b) Mode 1: Cov-SSI/CVA.

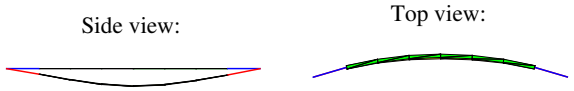

(c) Mode 2: numerical prediction.

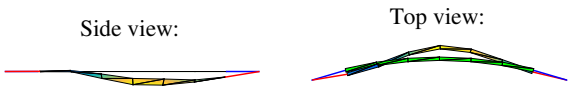

(d) Mode 2: Cov-SSI/CVA.

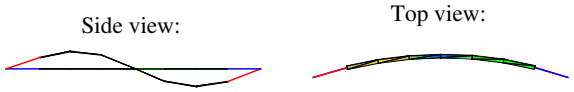

(e) Mode 3: numerical prediction.

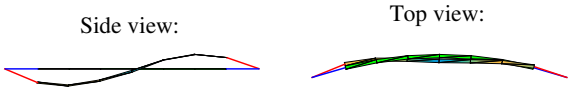

(f) Mode 3: Cov-SSI/CVA.

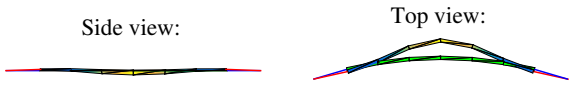

(g) Mode 4: numerical prediction.

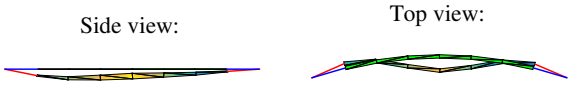

(h) Mode 4: Cov-SSI/CVA.

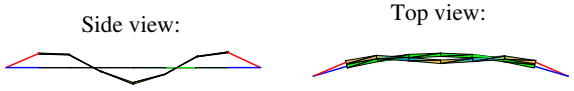

(i) Mode 5: numerical prediction.

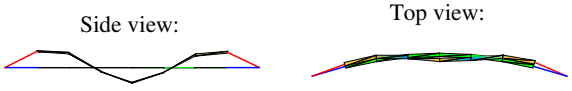

(j) Mode 5: Cov-SSI/CVA.

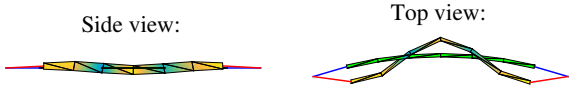

(k) Mode 6: numerical prediction.

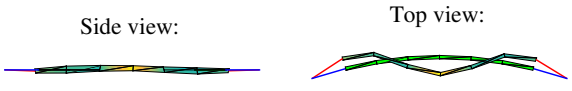

(l) Mode 6: Cov-SSI/CVA.

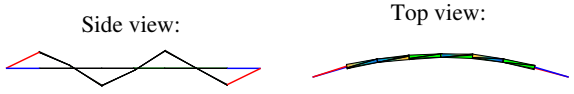

(m) Mode 7: numerical prediction.

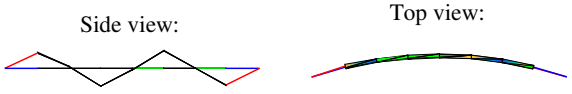

(n) Mode 7: Cov-SSI/CVA.

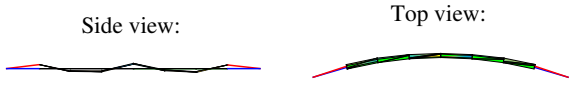

(o) Mode 8: numerical prediction.

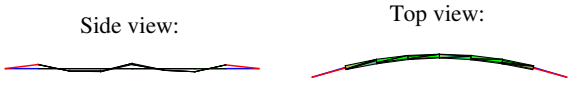

(p) Mode 8: Cov-SSI/CVA.

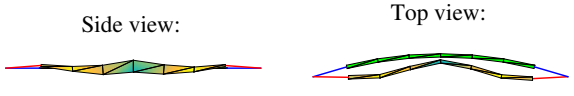

(q) Mode 9: numerical prediction.

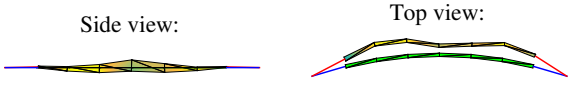

(r) Mode 9: Cov-SSI/CVA.

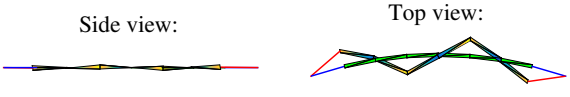

(s) Mode 10: numerical prediction.

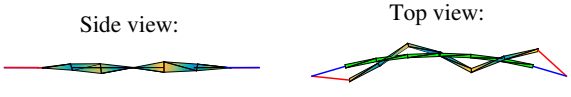

(t) Mode 10: Cov-SSI/CVA.

Figure 5: Mode shapes from eigenvalue solution of numerical prediction model and identified from Cov-SSI/CVA. The numbering refers to the numerical prediction.

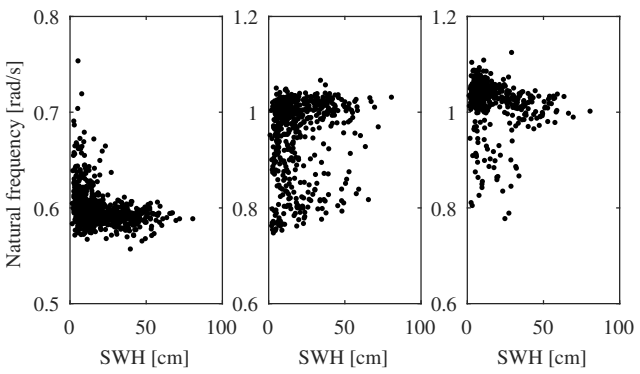

(a) Effect on natural frequency.

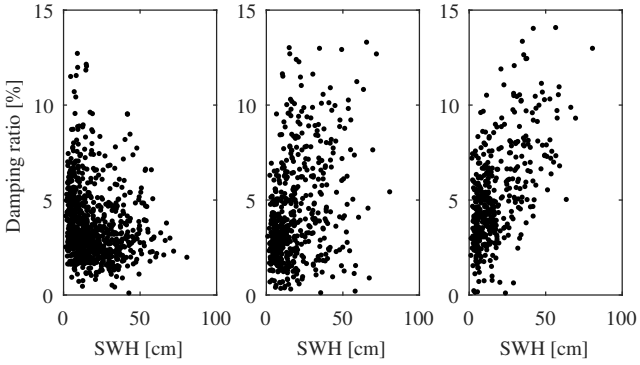

(b) Effect on critical damping ratio.

Figure 6: Effects on modal parameters from changing significant wave height.

Acknowledgements
The research was funded by the Norwegian Public Roads Administration. The authors gratefully acknowledge this support.

References

[1] E. Watanabe, "Floating bridges: past and present," *Structural Engineering International*, vol. 13, no. 2, pp. 128–132, 2003.

[2] J. M. W. Brownjohn, F. Magalhaes, E. Caetano, and A. Cunha, "Ambient vibration re-testing and operational modal analysis of the Humber Bridge," *Engineering Structures*, vol. 32, pp. 2003–2018, aug 2010.

[3] F. Magalhães, Á. Cunha, and E. Caetano, "Dynamic monitoring of a long span arch bridge," *Engineering Structures*, vol. 30, pp. 3034–3044, nov 2008.

[4] C. Farrar and G. James, "SYSTEM IDENTIFICATION FROM AMBIENT VIBRATION MEASUREMENTS ON A BRIDGE," *Journal of Sound and Vibration*, vol. 205, pp. 1–18, aug 1997.

[5] B. Peeters and G. De Roeck, "One-year monitoring of the Z24-Bridge: environmental effects versus damage events," *Earthquake Engineering & Structural Dynamics*, vol. 30, pp. 149–171, feb 2001.

[6] K. A. Kvåle, O. Øiseth, A. Rønnquist, and R. Sigbjörnsson, "Modal Analysis of a Floating Bridge Without Side-Mooring," in *Dynamics of Civil Structures, Volume 2*, vol. 2, pp. 127–136, Springer, 2015.

[7] K. A. Kvåle, O. Øiseth, and A. Rönnquist, "Operational modal analysis of an end-supported pontoon bridge," *Submitted*, 2016.

[8] K. A. Kvåle, R. Sigbjörnsson, and O. Øiseth, "Modelling the stochastic dynamic behaviour of a pontoon bridge: A case study," *Computers & Structures*, vol. 165, pp. 123–135, mar 2016.

[9] L. HERMANS and H. VAN DER AUWERAER, "MODAL TESTING AND ANALYSIS OF STRUCTURES UNDER OPERATIONAL CONDITIONS: INDUSTRIAL APPLICATIONS," *Mechanical Systems and Signal Processing*, vol. 13, pp. 193–216, mar 1999.

[10] G. H. Golub and C. F. Van Loan, *Matrix computations*, vol. 3. JHU Press, 2012.

[11] K. A. Kvåle and O. Øiseth, "Structural monitoring of an end-supported pontoon bridge," *Submitted*, 2016.